

# Piezoelectric, ferroelectric, optoelectronic phenomena in hydroxyapatite by first-principles and with various defects

V. S. Bystrov<sup>1\*</sup>, Jose Coutinho<sup>2</sup>, L. A. Avakyan<sup>3</sup>, A.V. Bystrova<sup>1,4</sup>,  
E.V. Paramonova<sup>1</sup>

<sup>1</sup>*Institute of Mathematical Problems of Biology, Keldysh Institute of Applied Mathematics, RAS,  
142290 Pushchino, Moscow region, Russia*

<sup>2</sup>*Department of Physics & I3N, University of Aveiro, Campus Santiago, 3810-193 Aveiro, Portugal*

<sup>3</sup>*Physics Faculty, Southern Federal University, Zorge Street 5, Rostov-on-Don 344090, Russia*

<sup>4</sup>*Institute of Biomedical Engineering and Nanotechnologies, Riga Technical University, Riga, Latvia*

\*Corresponding author, e-mail address: [vsbys@mail.ru](mailto:vsbys@mail.ru), [bystrov@impb.ru](mailto:bystrov@impb.ru)

Received 21 October 2019; accepted 2 December 2019; published online 19 December 2019

## ABSTRACT

The results are based on DFT calculations of hydroxyapatite (HAP) structures, pristine and defective, determined by various defects formed by Oxygen vacancy dependent on its charged states. Ordered hexagonal and monoclinic HAP phases have own spontaneous polarization, while disordered do not have it. These ferroelectric properties determined by orientation of OH dipoles provide piezoelectric and pyroelectric phenomena in such HAP structures for which all corresponding values and coefficients were investigated and calculated in this paper. The optical properties of defective HAP are mainly determined by various types of Oxygen vacancy defects (as well as hydroxyl OH group vacancy) and can lead to absorption and photocatalysis under ultraviolet illumination. The hybrid density functional theory (DFT) approaches of the structural and electronic properties of oxygen vacancies in large HAP supercells within the plane-wave formalism were mainly used in this work. The vacancies were investigated in large supercells, for which formation energies and electronic transition energies were calculated. The calculations were carried out using DFT, as implemented by the (Vienna ab initio package) VASP. The exchange-correlation potential was evaluated either using the generalized gradient approximation according to PBE functional or the three-parameter hybrid B3LYP functional, which incorporates a fraction of exact exchange with local and semi-local functional. These methods are also applied to the calculation of defect levels. Several other methods, such as AIMPRO and HyperChem, were used too, for several necessary cases and comparison. As a result, the main new features of pristine and defective HAP were established and analysed from first-principles.

## 1. INTRODUCTION

Hydroxyapatite (HAP) is an important natural and mineral component of mammal bones and teeth of vertebrates in humans and animals [1], which is used in prosthetic bio-implants [2]. Together with the organic bone's component (collagen) and living bone cells (osteoclasts, osteoblasts and osteocytes) [1–4] HAP crystallizes as an array of

stand-alone HAP platelet compositions or needle-like nanocrystals in the gaps of laid tropocollagen fibrils, forming and strengthening the bone structure [4-7]. Due to its natural innate biological activity, HAP is widely used in medicine for manufacturing bone and dental implants (both filler and coating material for titanium and similar implants) [2-5], for bone replacement and regeneration [1-8]. However, despite the importance of HAP in medicine, several promising

new applications of this material (e.g., in photocatalysis [9]), depend on how well we understand its fundamental properties.

HAP has specific structural features that determine its basic physical properties, charge distribution, and surface electric potential, which play a particularly important role in the adhesion and proliferation of living cells [1-8]. A distinctive feature of HAP is that it has a specific direction of the formation of hydroxyl OH groups (internal OH channels) along the *c* axis, which allows protons to be transported along this axis under special conditions [5, 8, 10, 11]. Formation of internal polarization along these OH channels creates a directional distribution of surface charge density. This is very important for the adhesion of living cells, their growth and proliferation.

Constantly growing interest of researchers to the studies of hydroxyapatite in the world shows that this material has a unique complete of physical properties. Several years ago it was considered only as a structure of a centrosymmetric crystal, but by now it has been established that it has noncentrosymmetric structural properties [12-17]. Recent studies have shown that HAP exhibits both piezoelectric, pyroelectric and, in whole, ferroelectric properties [8, 12-17]. A number of theoretical studies of the structure and properties of HAP have been carried out [18-21]. They showed the value of the  $d_{33}$  piezoelectric coefficient  $\sim 16$  pC/N [20] which is in good agreement with the experimental study as described in [15, 17]. And, in addition, it turns out that HAP has important photocatalytic properties [22-24]. This is due to the electronic features of existing defects in HAP, especially due to oxygen vacancies [24]. Further, experimental evidence suggests that oxygen vacancies play a critical role in the production of surface radicals upon exposure of HAP to ultraviolet (UV) light. However, very little is known about the underlying physical and chemical details for these processes in the HAP. Moreover, in various fields of application HAP demonstrates different properties. So, for example, it turned out that its polar properties are important for biomedicine and implantology.

In this article, we analyze the polarization values obtained for various HAP models and the calculation methods used [8, 18-21, 24-29] in comparison with various experimental data [11-17,

20, 21, 30, 31]. All relevant ferroelectric effects are also evaluated and analyzed: piezoelectric and pyroelectric coefficients were estimated and compared [21]. Optical properties, in particular photocatalytic properties, which are especially affected by defects such as oxygen vacancies with various charges and structural features, are also taken into account [25, 26].

For all these aims the novel developments of the hybrid density functional theory (DFT) in the structural and electronic properties of oxygen vacancies in large HAP supercells within the plane-wave formalism [25, 26] were mainly used in this work. The vacancies were investigated in large supercells, for which formation energies and electronic transition energies were calculated. The calculations were carried out using DFT, as implemented by the (Vienna ab initio package) VASP [28]. The exchange-correlation potential was evaluated either using the generalized gradient approximation according to PBE functional or the three-parameter hybrid B3LYP functional, which incorporates a fraction of exact exchange with local and semi-local functional [25]. These methods are also applied to the calculation of defect levels [26]. Several other methods, such as AIMPRO [27] and HyperChem [29], were used too, for several necessary cases and comparison. As a result, the main new features of pristine and defective HAP were established and analysed from first-principles.

## 2. COMPUTATIONAL DETAILS AND MODELS

The calculations of pristine and defective HAP structures and properties were carried out from first principles using DFT by AIMPRO code (in Local Density Approximation (LDA)) [27] and by VASP [28] (in Generalized Gradient Approximation (GGA) according to Perdew, Burke, Ernzerhof (PBE) approach and with Becke three-parameter (B3LYP) hybrid functional [25, 26]) in combination with semi-empirical quantum-chemical (QM) PM3 method from HyperChem 8.0 package [29]. More computational details are described in [25, 26]. The main peculiarity of this study is the introduction of the supercells model made up of  $2 \times 2 \times 2 = 8$  polar HAP unit cells (space group  $P6_3$ ) for hexagonal HAP phase both for pristine and defective HAP with oxygen vacancies. The monoclinic phase

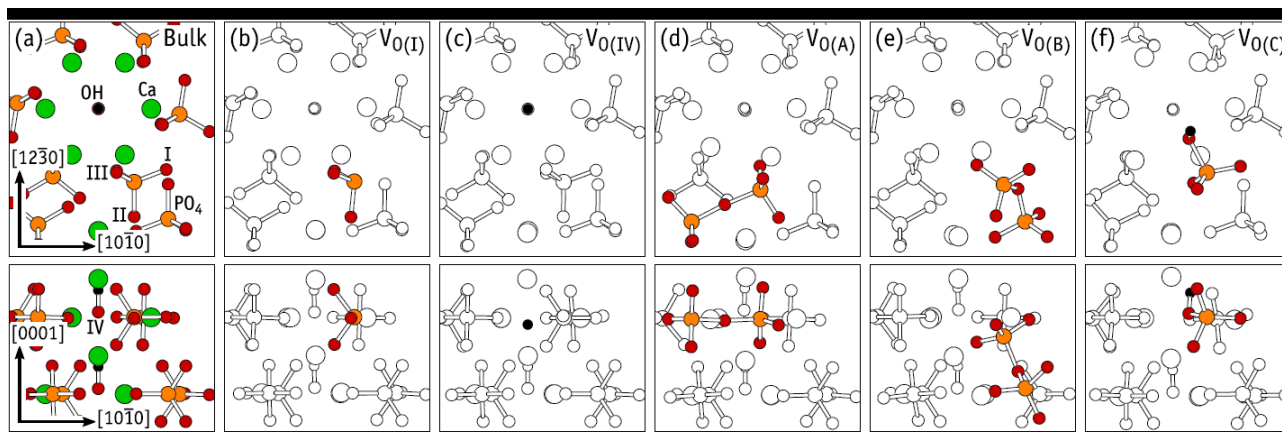


Figure 1. Atomic diagrams showing the structure of a pristine region of HAP (Bulk), along with structures I, IV, A, B and C of  $V_O$  defects. Upper and lower insets correspond to the same structures viewed along  $[0001]$  and  $[12\bar{3}0]$  directions of the hexagonal lattice, respectively. On the bulk diagrams, Ca, P, O and H atoms are shown in green, orange, red and black, respectively. The four different oxygen sites are indicated with I, ..., IV labels. On defect diagrams, only atoms neighbouring the defect are coloured. (Adapted and modified with permission from [26]. Copyright (2019) American Chemical Society).

$P2_1/b$  is more stable, but it differs a little only by 25 meV per unit cell [19], with their electronic structures being the same. Crystalline HAP has oxygen atoms on four symmetry inequivalent sites, which are referred to as oxygen types I–IV. Types I, II, and III are in the phosphate units, while type IV oxygen atoms are located in the  $\text{OH}^-$  anions. These are denoted as  $\text{O(I)}$ , ...,  $\text{O(IV)}$  (oxygen vacancy  $V_O(\text{I})$ , ...,  $V_O(\text{IV})$ , Fig. 1) and they were analysed in [26]. In all these calculations we take account of full relaxation of the cell, including adjusting the atomic positions and the cell shape (total optimization of the structure). But, a full relaxation of such large HAP supercells (as  $2 \times 2 \times 2 = 8$  polar HAP unit cells) using plane-wave hybrid-DFT is prohibitively expensive. Instead, defect structures were first found by relaxing all atomic coordinates within PBE (it is step 1 of calculations). The resulting structures were used at the second step (step 2 of calculations), where the total energy was obtained within hybrid-DFT by means of the B3LYP single-point calculation. This procedure was necessary due to the sheer size of the Hamiltonian at hand combined with the use of a plane-wave method. All defect calculations employed a  $\Gamma$ -point sampling [25, 26]. The optimized data obtained for each HAP structure, were taken out and transformed to a format of HyperChem files [29] for calculations of their physical properties, particularly, polarization. For

present calculations we use semi-empirical quantum mechanics methods PM3 method in restricted and unrestricted Hartree-Fock approximation (RHF/UHF).

### 3. MAIN RESULTS AND DISCUSSIONS

Recently computed data show, first, that HAP can co-exist in different phases: hexagonal and monoclinic [8, 19]. Now we are especially interested in an ordered hexagonal structure, which could demonstrate piezoelectric and pyroelectric properties as well [20, 21]. For instance, the energy difference between HAP unit cells with  $P6_3$  and  $P6_3/m$  symmetry (the latter being obtained by aligning the OH units along opposite directions in their big supercell model) is  $E(P6_3/m) - E(P6_3) = 0.39$  eV with both energies being obtained from fully relaxed B3LYP-level calculations [26]. This result is in line with computed difference  $E(P6_3/m) - E(P6_3) = \sim 0.132$  eV/unit cell in LDA approximation [19].

#### 3.1. Polarization and following piezo-electric and pyro-electric - ferroelectric effects

To calculate the polarization for different HAP phases we construct simplest models, including mainly the OH-channels with various orientations of the OH dipoles (see on Fig. 2). Table 1 present polarization data obtained by calculations of these

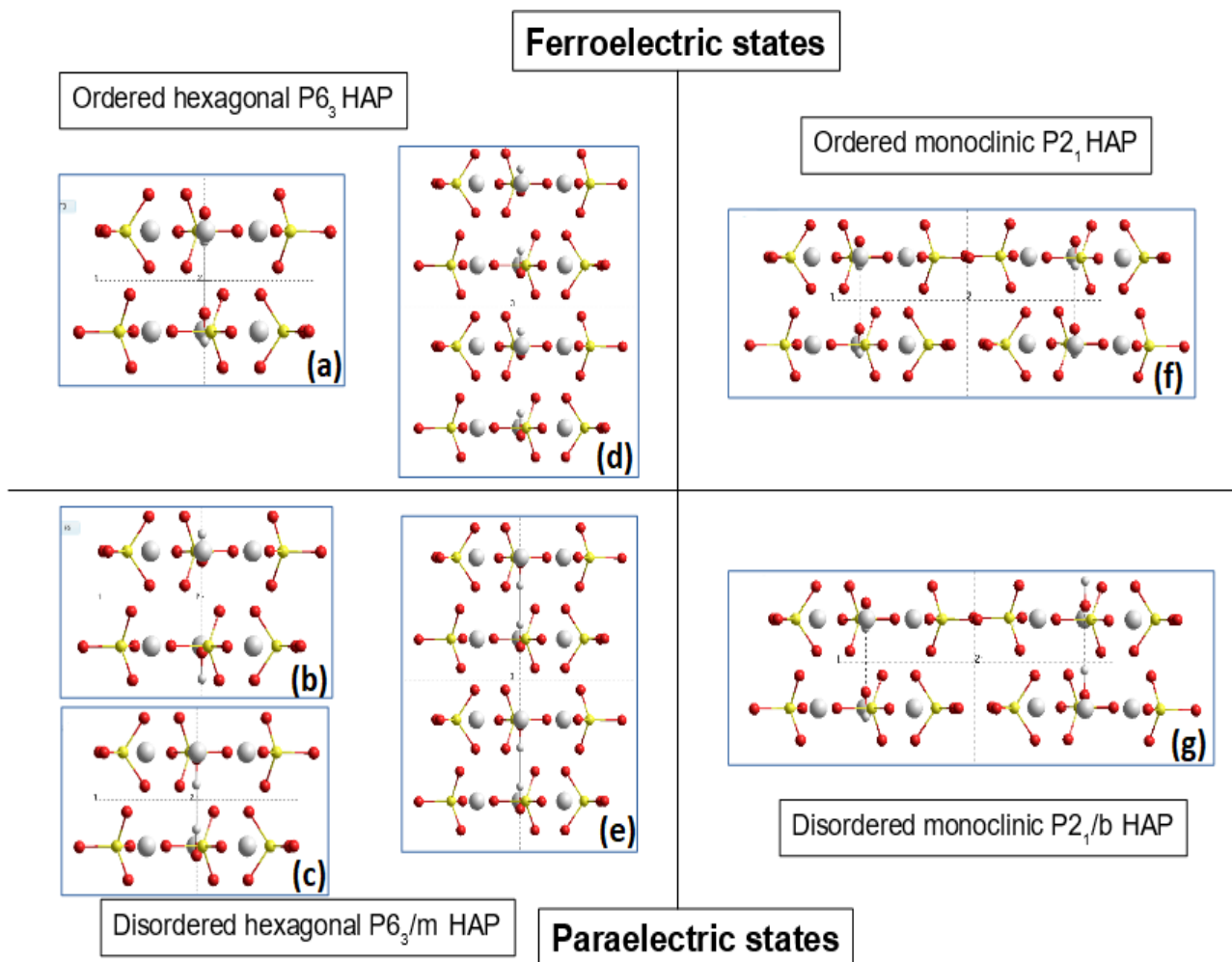


Figure 2. Schematics of OH electric dipole orientation and switching from paraelectric (disordered) to ferroelectric (polar and ordered) states of the hexagonal and monoclinic HAP:

- a), d) – 1 and 2 units  $P6_3$  polar ordered model with parallel orientation of the OH dipoles;  
 b), c) and e) – 1 unit models with various ant-parallel 11 and 22 (opposite) OH dipoles orientation, and 2 units -  $P6_3/m$  model;  
 f), g) – monoclinic polar ordered polar  $P2_1$  and disordered non-polar  $P2_1/b$  models.

models in comparison with other data.

The data obtained by these calculations in comparison with other data computed and measured for HAP polarization values in their different phases clearly show, that namely ordering of the OH dipoles determine the existing of the polar HAP phase (with total sum of polarization directed along the OH-channel and coincides with c-axis) and its switching between paraelectric (disordered hexagonal  $P6_3/m$ ) and ferroelectric (polar and ordered hexagonal  $P6_3$ ). The

polarization values in the ferroelectric phase for different approaches are comparable and are of the order of  $P \sim 0.02 - 0.12 \text{ C/m}^2$  (Table 1), while in paraelectric (non-polar) phase all different models show values close to zero, due to compensation of an opposite anti-parallel orientation of OH groups along these OH-channels, but it is not equal exactly  $P = 0$ . It has some deviation around zero sum of total polarization by a several small values  $\sim 0.001 \text{ C/m}^2$ , that arise due some local fluctuations in the atomic positions and the OH dipole orientations.

Table 1. Polarization in HAP calculated by PM3 method after VASP in comparison with other data

	Model/Method/ Space Group		Hexagonal RHF, C/m <sup>2</sup>		Hexagonal UHF, C/m <sup>2</sup>		Monoclinic RHF, C/m <sup>2</sup>		Other data refs
			Pz	Pt	Pz	Pt	Pz	Pt	
1 unit model	OH-OH par1	P6 <sub>3</sub>	<b>0.0111</b>	<b>0.031</b>	<b>-0.030</b>	<b>0.107</b>			
	HO-HO par3	P6 <sub>3</sub>	<b>-0.011</b>	<b>0.029</b>	<b>-0.054</b>	<b>0.118</b>			
	OH-HO 22	P6 <sub>3</sub> /m	-0.004	0.005	0.002	0.002			
	HO-OH 11	P6 <sub>3</sub> /m	-0.001	0.002	0.001	0.002			
2 unit model	OH-OH par 0	P6 <sub>3</sub> P2 <sub>1</sub>	<b>0.02</b> -	<b>0.027</b> -	<b>-0.075</b> -	<b>0.127</b> -	- <b>-0.020</b>	- <b>0.064</b>	
	OH anti- par 1	P6 <sub>3</sub> /m P2 <sub>1</sub> /b	0.0012 -	0.013 -			- -0.004	- 0.006	
	OH anti- par 2	P6 <sub>3</sub> /m	-0.001	0.011					
Various method (for ordered HAP)	AIMPRO par	P2 <sub>1</sub> P6 <sub>3</sub>	- <b>-0.018</b>	-			<b>-0.021</b> -	-	Bystrov [20, 21], using HyperChem /AIMPRO
	VASP	P6 <sub>3</sub> P2 <sub>1</sub>	<b>-0.0705</b> -				- <b>-0.0987</b>		Shunbo Hu, et al [31]
	HyperChem		<b>~ 0.046 – 0.112 (up ~ 0.18)</b>						Bystrov et al. [18, 35]
	Experimental		<b>Up to ~ 0.149</b>						Nakamura et al [11]
	AFM Experim.		<b>From 0.005 up to ~ 0.072</b>						Vandiver et al [32]
	Experim. vary		<b>~ 0.1 – 0.2</b>						Lang, Tofail et al [12-17]

\*) Here “par” denotes ‘parallel’ orientation of OH group (dipoles), “anti-par” - “anti-parallel”

Note, that the accuracy of these calculations was determined by the convergence limit at the level of ~ 0.001 (due to HyperChem software option [20, 29] for the PM3 method calculations).

The monoclinic phase P2<sub>1</sub>/b (disordered and paraelectric) is a little more stable (than P6<sub>3</sub>/m), but it differs only on 25 meV per unit cell [21] (as mentioned above). The similar relation as for hexagonal phases is existing between of the ordered polar monoclinic HAP phase with P2<sub>1</sub> space group and disordered HAP phase with anti-

parallel OH dipoles orientation in P2<sub>1</sub>/b space group. All these relations are shown on the schematics presented on Fig. 2 and Table 1.

This effect may be due to restriction of the models, but may reveal some nonsymmetrical HAP structures. In any case, it is well known that a full ideal periodical crystal structure for HAP does not exist in real nature. More or less all HAP structures have many deviations from an ideal crystal: non-stoichiometry, replacements, insertions, vacancies etc. Especially important role belongs to oxygen

vacancies of different types [26]. We consider some results of the influence of such defects below.

But for all ordered HAP structures, as pristine as well defective, the existence of such spontaneous polarization led (as in any ferroelectric) to the pyroelectric and piezoelectric phenomena. Now the values of the piezoelectric coefficients are well known and are determined by calculations and measurements  $d_{33} \sim 6.4 - 8.5$  pm/V (or pC/N) for hexagonal  $P6_3$  HAP, and of the order of  $d_{33} \sim 15.7 - 16.5$  pm/V (or pC/N) for monoclinic  $P2_1$  HAP [15-17, 20, 21, 30]. For the values of pyroelectric coefficients, the estimation for the HAP in the hexagonal phase yields the value 10–100  $\mu\text{C}/(\text{m}^2\text{K})$ , which is in line with experimental observations ( $\rho \sim 12 \mu\text{C}/(\text{m}^2\text{K})$ ) [14-17].

It is interesting to note, first, that recent calculations of polarization in HAP by first-principle method and using VASP in work [31] yielded the values which are very close to our data, second, that in work [32] the HAP surface charges density was experimentally measured by atomic force microscopy (AFM) using special functionalized tips. It turned out to have similar values.

### 3.2. Electronic and optical properties acting by defect energy levels in HAP

The most basic property of a periodic solid is its fundamental energy gap  $E_g = E_c - E_v$  (where  $E_c$  – is the conductive band bottom,  $E_v$  – is the valence band top), which is positive for semiconductors and insulators. This  $E_g$  dominates many properties. The fundamental energy gap of a periodic solid characterizes low-energy single-electron excitations. Band-gap problem in Kohn-Sham density functional theory is that the gap in the band-structure of the exact multiplicative Kohn-Sham (KS) potential substantially underestimates the fundamental gap. To avoid this problem the generalized KS theory (GKS) is developed, in which the band gap of an extended system equals the fundamental gap for the approximate functional if the GKS potential operator is continuous and the density change is de-localized when an electron or hole is added. In this case GKS band gaps from meta-generalized gradient approximations (meta-GGAs) and hybrid functionals can be more realistic

than those from GGAs or even from the exact KS potential [25, 26].

For the case of one electron excitation, the following relations can be used: Ionization energy  $I = E(+1) - E(0) = -E_v$ , electron affinity  $A = E(0) - E(-1) = -E_c$ , and fundamental gap  $E_g = I - A = E_c - E_v$ , while the KS band edges are  $\epsilon_{HO}$ ,  $\epsilon_{LU}$  (where the Highest Occupied (HO) and Lowest Unoccupied (LU) mark the corresponding electron energy states), and corresponding band gap is equal  $\epsilon_g = \epsilon_{LU} - \epsilon_{HO}$ , in the PBE (step 1) and B3LYP (step 2) for calculations on the same  $2 \times 2 \times 2$  B3LYP lattice of HAP super-cell (HAP8). As a result, the values of magnitude  $(I + A) / 2$ , the energy difference from the gap centre to the vacuum level, depend only slightly on the approximation. For the case of our HAP  $P6_3$  supercell model (in pristine bulk crystal), these relations computed using VASP [28], are presented in Table 2.

Defect HAP structures with oxygen vacancies  $V_O$  described above [26] were investigated in neutral, positive, and double positive charge states. For double positive charge states, new structures referred to as extended (or bridge) structures, were also found for the oxygen vacancy in HAP [26]. One type of extended structures can be described as a pair of neighbouring oxygen vacancies connected by O bridge,  $2V_O + O$ . A second type is described as a complex consisting of OH-vacancy next to an H-interstitial,  $V_{OH} + H$ . Two defects of type  $2V_O + O$  are singled out and labelled  $V_O(A)$  and  $V_O(C)$ . One  $V_{OH} + H$  defect is referred to as  $V_O(B)$ . The structures types and stability of  $V_O$  defects strongly depend on the charge states [26]. For neutral and single positive cases,  $V_O(I) - V_O(IV)$  are stable. For charge states, extended configurations ( $V_O(A) - V_O(C)$ ) relax to  $V_O(I) - V_O(IV)$  structures. If charges +2, structures  $V_O(I) - V_O(IV)$  are unstable and relax to extended structures (see Fig.1).

Inspection of KS eigenvalues for  $k = \Gamma$  confirmed that  $V_O$  defects are all donors. Figure 3 shows the B3LYP Kohn-Sham (KS) energies of neutral vacancies  $V_O$  in the energy range of one-electron band gap  $\epsilon_{cb} - \epsilon_{vb} = 7.34 \text{ eV} \sim \epsilon_g = \epsilon_{LU} - \epsilon_{HO}$ . Here,  $\epsilon_{cb}$  and  $\epsilon_{vb}$  are energies of the bottom and top of the conduction band and valence band, respectively, and correspond to KS band edges  $\epsilon_{HO}$ ,  $\epsilon_{LU}$ . These are represented by solid horizontal

lines spanning the whole diagram width. The short horizontal lines represent the defect-related states, as obtained from the KS eigenvalues. Level occupation is indicated by upward and downward arrows. The value of  $\epsilon_{cb}$  is the origin of the energy scale.

Although the Kohn–Sham band structure lacks any physical significance, we can always make use of Koopmans' theorem to connect the highest occupied state to the photoionization energy of the system under scrutiny [26]. With this in mind, it is evident that the simpler  $V_O(I)$ – $V_O(IV)$  structures are deep donors with photoionization energies close to 6 eV, while semi-vacancy configurations (extended

or bridge vacancy defects, which joined two molecular groups - see Fig. 1 d, e, f) are shallower donors, where promotion of electrons to the conduction band requires a low ionization energy. This makes these complex defects  $V_O(A)2+$ ,  $V_O(B)2+$ , and  $V_O(C)2+$  (with charge  $q=+2$ ) rather stable species. (The details of its formations are given below).

As regards the cases of the oxygen vacancies  $V_O(I)$ – $V_O(IV)$  with neutral charge  $q=0$  and charge  $q=+1$  (Fig.1, b, c), the same two-step DFT calculations of various defective HAP structures in our supercell model of hexagonal  $P6_3$  group show that all the levels are double occupied by electrons

Table 2. Energy characterization of pristine bulk HAP8 (2x2x2) calculations in the main state.

Method	$(I + A)/2$ , eV	$I = -E_v$ , eV	$\epsilon_{HO}$ , eV	$A = -E_c$ , eV	$\epsilon_{LU}$ , eV	$E_g$ , eV	$\epsilon_g$ , eV
PBE	-4.598094	-1.979512	1.9801	-7.216676	7.2232	5.237165	5.2431
B3LYP	-4.395551	-0.971008	0.7259	-7.820094	8.0662	6.849086	7.3403

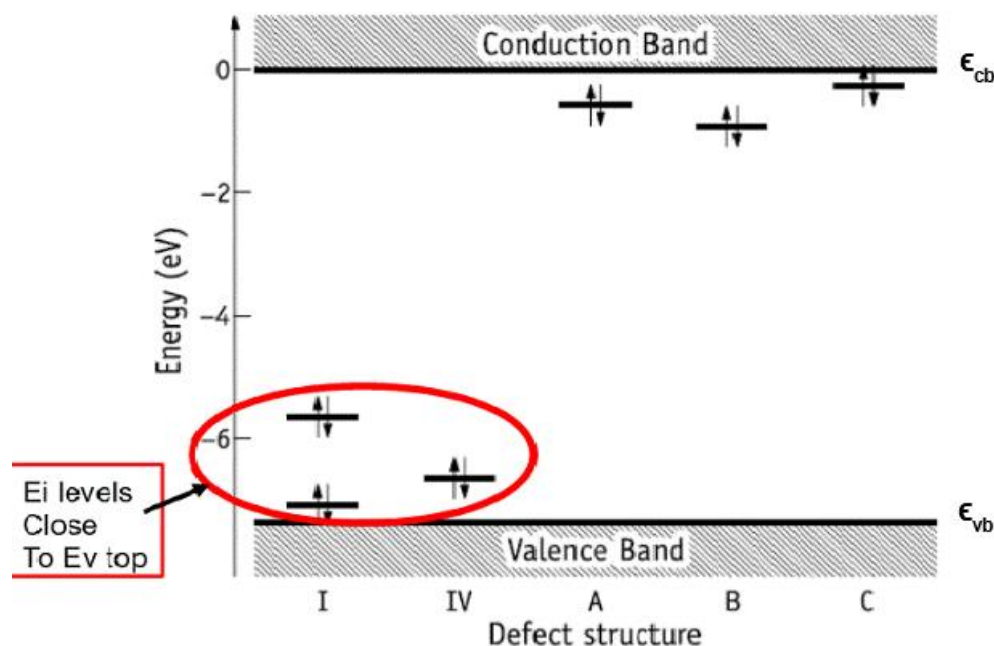


Figure 3. Kohn–Sham energy levels of neutral  $V_O$  defects in a HAP supercell at the  $k = \Gamma$  point. The defect structure I is also representative of structures II and III (see text). The latter have gap states that deviate from those of  $V_O(I)$  by less than 0.2 eV [26]. (Reprinted and modified with permission from [26]. Copyright (2019) American Chemical Society).

Table 3. Energy levels for A0 (Vo(I)–Vo(III) from 3 phosphate group) and D0 (Vo(IV) from hydroxyl group) (with double occupied by electron energy levels).

Defect	Method	$E_c = \varepsilon_{LU}$ , eV	$E_v^* = \varepsilon_{HO}^*$ , eV	$E_g = \varepsilon_{LU} - \varepsilon_{HO}^*$ , eV	$E_i = \varepsilon_{HO}$ , double occupied, eV	$E_{g-opt} = E_c - E_i$ , eV	$E_i - E_v^*$ , eV
A0 = A <sup>0<sub>I</sub></sup> (Vo(I) )	PBE	7.2208	2.1732	5.0476	3.3248	3.8960	1.1516
	B3LYP	8.0624	1.0127	7.0497	2.4418	5.6206	1.4291
A0 = A <sup>0<sub>II</sub></sup> (Vo(II) )	PBE	7.2231	2.0341	5.189	3.3606	3.8624	1.3265
	B3LYP	8.0640	0.8329	7.2311	2.4841	5.5799	1.6512
A0 = A <sup>0<sub>III</sub></sup> (Vo(III) )	PBE	7.2211	2.1049	5.1162	3.4816	3.7395	1.3767
	B3LYP	8.0619	0.9286	7.1333	2.6131	5.4488	1.6845
D0 = D <sup>0</sup> (Vo(IV) )	PBE	7.2514	1.9646	5.2868	2.3930	4.8583	0.4284
	B3LYP	8.0946	0.7104	7.3842	1.4451	6.6495	0.7347

and all the data obtained for their KS energies are more close to the valence band top (these cases are presented in Table 3).

It must be noted that the energy of the highest occupied states in Figure 3 accounts for vertical transitions which are in principle accessible by optical excitation. However, transition levels (or electronic levels) of defects are equilibrium properties and must be derived from the formation energy of both ground states involved in the transitions. This is analogous to the zero-phonon (ZP) line energy in photo-luminescence/absorption experiments. Hence, the energy of a transition level of a defect will differ from the vertical (optical) transition by a Franck–Condon relaxation energy.

Usually the formation energy of a defect in a crystalline sample (with arbitrary volume) can be written as [33]:

$$E_f = E(q, R) - E_{HAP} - \sum_i \Delta n_i \mu_i + q(E_v + E_f) \quad (1)$$

which depends primarily on the energy difference between defective and pristine crystals, namely,  $E$  and  $E_{HAP}$ , respectively. The defect is considered on a particular configuration  $R$  and charge state  $q$ . The third and fourth terms account for any stoichiometric and charge imbalances between the

first two terms. Accordingly,  $\mu_i$  are chemical potentials for any species  $i$  which are respectively added ( $\Delta n_i > 0$ ) or removed ( $\Delta n_i < 0$ ) from or to the perfect crystal to make the defect. The last term accounts for the energy involved in the exchange of electrons between the defect in charge state  $q$  and an electron reservoir with a chemical potential  $\mu_e = E_v + E_f$ , where  $E_v$  and  $E_f$  stand for the energy of the valence band top and Fermi level, respectively. The latter mostly depends on the type and amount of defects and impurities in the crystal and can vary in the range  $0 \leq E_f \leq E_g$ , where  $E_g$  is the band gap width of the material.

This eq. (1) allows us to construct a phase diagram for the oxygen vacancy in HAP as a function of the chemical potentials and Fermi energy. In recent work [26] such calculations and analysis of the stability of some concrete species were carried out. It was shown that [26], the value of  $E_f$ , for which two solutions  $E_f(q)$  and  $E_f(q + 1)$  from eq. (1) become identical, defines a threshold above which  $Vo^q$  is more stable than  $Vo^{q+1}$ .

The defect transition level for two various charged states  $E_f(q)$  and  $E_f(q+1)$  can be calculated with respect to the valence band top  $E_v$  as

$$E(q/q+1) - E_v = [E(q, R^q) - E(q+1, R^{q+1})] - I_{bulk} \quad (2)$$

where different structures  $R^q$  and  $R^{q+1}$  have different charges  $q$  and  $q + 1$ ,  $E$  is the total energy (including charge correction for  $q \neq 0$ ),  $I_{\text{bulk}} = E_{\text{bulk}}(q = +1) - E_{\text{bulk}}(q = 0)$  is the ionization energy of a bulk supercell.

One could have replaced  $I_{\text{bulk}}$  in (2) by the energy of the highest occupied KS energy level from a bulk calculation. We have chosen to avoid the use of Kohn–Sham energies, keeping the results solely based on total energies. The KS band gap from B3LYP-level calculations ( $E_g^{\text{KS}} = 7.34$  eV) is about 0.49 eV wider than the quasi-particle gap (calculated as  $E_g^{\text{QP}} = E_{\text{bulk}}(+1) + E_{\text{bulk}}(-1) - 2E_{\text{bulk}}(0) = 6.85$  eV) [26].

In Table 4 the calculated transition levels,  $\Delta E(q/q + 1) = E(q/q + 1) - E_v$  involving the relevant structures  $R^q$  and  $R^{q+1}$  are presented. Results based on both PBE and B3LYP functionals are reported. It is evident that PBE results have error bars of at least 1 eV, which is in line with our findings reported in [25].

As everyone can see, the position of these energy levels is not much different (especially for the PBE calculations), although in the case of B3LYP these levels are slightly higher than the  $E_v$  for the direct case. In any case, these deviations are within 1 eV.

It is also important to note that such levels close

to the top of the valence band were recently observed by the photoelectron emission spectroscopy experiments, and the photoelectron work function from HAP was measured for different external actions [23, 34]. Moreover, it was noted in the work [34] that they may occur during a number of actions on HAP samples (heating and annealing, gamma irradiation, microwave effects and combined hydrogenation with microwave irradiations). It is in these cases that the formation of a sufficiently large number of oxygen vacancies is possible, especially in the OH group, with the lowest energies relative to the top of the valence band (see Tables 3 and 4).

Another important feature is the fact that single defects with positive charge are not stable. Considering the lowest energy structures for each charge state, it is possible to find that a transition level from  $q=0$  to  $q=+2$  ( $0/2+$ ) is at the crossing point. The location of the level was calculated at  $E(0/2+) - E_v = 2.65$  eV [26].

Hence, for p-type HAP, where the Fermi energy is at the lower-half of the gap, oxygen vacancies are likely to adopt double positive extended structures  $V_o(B)^{2+}$  or  $V_o(C)^{2+}$ . Conversely, in n-type (and intrinsic) HAP, the neutral state is more stable and the defect will be found as an isolated  $H^-$  hydride in the OH-channel (i.e.,  $V_o(IV)^0$ ) [26].

Table 4. Calculated Electronic Donor Levels of  $V_o$  in HAP with Respect To the Valence Band top,  $\Delta E(q/q + 1) = E(q/q + 1) - E_v$ . (Reprinted and adapted with permission from [26]. Copyright (2019) American Chemical Society.).

Functional	$\Delta E(0/+)$ , eV	$R^0/R^+$	$\Delta E(+/2+)$ , eV	$R^+/R^{2+}$
PBE	1.53	I/I	1.71	I/A
B3LYP	2.51		2.60	
PBE	1.58	II/II	2.64	II/B
B3LYP	2.50		3.74	
PBE	1.72	III/III	2.59	III/C
B3LYP	2.72		3.60	
PBE	0.17	IV/IV	3.08	IV/B
B3LYP	0.99		3.94	

Table 5. Main energy relations for HAP with D defects, when Oxygen vacancy is in OH ( $V_{O(IV)}$ ), with Respect To the Conduction Band bottom  $\Delta E(q/q+1) = E_c - [E(D^0) - E(D^+)]$ , (all data are in eV units).

Method	$E_c - [E(D^0) - E(D^+)]$	$\Delta E(D^0/D^{0+1e}) = E(D^0) - E(D^{0+1e})$	$E_{abs}$	$E_{FC(+)}$	$E_{lum}$	$E_{FC(0)}$	$E_{abs} - E_{lum} = E_{FC(+)} + E_{FC(0)}$
PBE	4.927566	2.009449	5.207227	0.279661	3.379735	1.547831	1.827492
PBE on B3LYP lattice	5.071172	2.016323	5.200354	0.129182	3.518707	1.552465	1.681647
B3LYP	5.856286	1.963808	6.671180	0.814895	4.169527	1.686760	2.501654

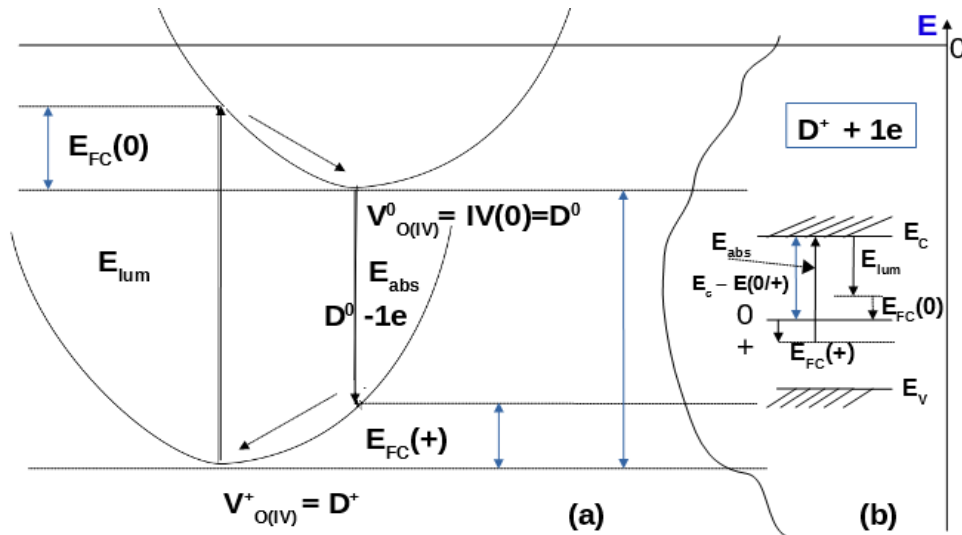


Figure 4. Schematics of the Franck-Condon relaxation processes: a) in direct energies changes during excitation / luminescence with corresponding lattice relaxation of atomic positions shifting; b) the corresponding energy band scheme with relation to  $E_c$  and  $E_v$  with  $E_g = E_c - E_v$ .

For Frank-Condon (FC) relaxation we must estimate the structure and energy changes during excitation/luminescence processes. In this case, similarly to eq. (2) we can calculate the defect transition level for two various charged states  $E_i(q)$  and  $E_i(q+1)$  with respect to the conduction band bottom  $E_c$ . By way of example we consider the case of  $V_{O(IV)}$  vacancy in our HAP  $P6_3$  supercell model. In this case we can write

$$E_c - E(D^0/D^+) = A_b - [E(D^0) - E(D^+)] = A_{bulk} - [E(V_{O^{q=0}(IV)}) - E(V_{O^{q=+1}(IV)})], \quad (3)$$

where  $A_{bulk} = E_{bulk}(q=0) - E_{bulk}(q=-1)$  is the electron affinity energy of a bulk supercell.

The main relaxation and processes in this case are shown in Fig. 4 and the data are presented in Table 5.

We must emphasize the difference between direct energy calculations from VASP data and the energies computed by relation (1) between energy of the defective and pristine crystals, with taken into account some stoichiometric and charge imbalances between them and the chemical potentials for any interacting species. As a result, the absorption and luminescence energies have

more correct values for solid states case. The relations obtained for FC relaxation in both cases (absorption and luminescence) have good and quite correct values for all approaches (see Table 5 last column).

#### 4. CONCLUSIONS

Using various computational approaches developed we demonstrate that the ordered HAP hexagonal (space group  $P6_3$ ) and monoclinic (space group  $P2_1$ ) phases have strong own (spontaneous polarization) of the order of  $P_s \sim 0.05 - 0.15 \text{ C/m}^2$ , which is determined by parallel orientation of the OH group dipoles (with some variations depending from structural and environmental conditions), while disordered hexagonal and monoclinic phases have close to zero polarization  $P < 0.001 \text{ C/m}^2$ , due to anti-parallel orientation of OH dipoles, that compensate one another. This behavior has a ferroelectric nature in whole. As a result, both ordered HAP phases have piezoelectric coefficients of the order of  $\sim 6.4 - 16.5 \text{ pm/V}$  (which vary between these phases), and pyroelectric coefficients  $p \sim 10-100 \text{ mC/(m}^2\text{K)}$ , that are confirmed by many experimental data.

Optical properties of the defective HAP are determined by various defects formed by Oxygen vacancies, depending on charges state. Defect HAP structures with oxygen vacancies can be in neutral, positive, and double positive charge states. For double positive charge states new structures referred to as extended (or bridge) structures, were established in HAP.

We found that the vacancies essentially occur in such two distinct forms, either as a simple vacant oxygen site (referred to as structures I-IV), or as an oxygen atom replacing two neighbouring oxygen vacancies (bridge or extended structures named as "A-C"). The former type of vacancies is deep donors, while the latter are shallow donors with rather low ionization energies. No acceptor states (stable negatively charged defects) were found. Vacancy structures I-IV are more stable in the neutral charge state, while bridge structures A-C are preferred in the double plus charge state. This means that the oxygen vacancy adopts rather different configurations on samples where the

Fermi energy is in the upper or the lower half of the band gap. From inspection of the one-electron Kohn-Sham levels, combined with the transition levels obtained from total energies, we find that electron promotion from the valence band top to the donor state of the positively charged structures, involves a zero-phonon absorption of 3.6-3.9 eV.

This transition leads to a spontaneous breaking of either a P-O bridge-bond or an O-H bond, and most likely explains the 3.4-4.0 eV absorption onset for the observation of photocatalysis under persistent UV illumination. The structure's types and stability of defects strongly depend on the charge states. Inspection of the Kohn-Sham eigenvalues at  $k = \Gamma$  confirmed that neutral Oxygen vacancy defects are all donors involves the luminescence and absorption of 3.6-3.9 eV.

Further development and more accurate calculation of these electronic properties and optical photoexciting and photocatalytic processes can be made by correct calculations of the electron-electron correlation of the excited electron states taking into account the Frank Condon relaxation. These contributions are calculated for the case of the  $V_{O(IV)}$  vacancy in our HAP  $P6_3$  supercell model and their results showed that FC shift obtained has reasonable values (for electron excitation  $\sim 0.2 \text{ eV} / 0.8 \text{ eV}$  in PBE/B3LYP, and for luminescence  $\sim 1.6 \text{ eV} / 1.8 \text{ eV}$  in PBE/B3LYP). These investigations will be continued for other oxygen vacancy types.

However, we must conclude that for any case, irrespective of these FC relaxation processes, the formation of the various types defects in HAP through different oxygen vacancies gives rise to an opportunity of the photo-excitation processes in the close ultraviolet (UV-C) and visible light region. These photo-excitation effects obviously produce the photo-catalytic activity of HAP. One only needs to introduce a sufficient amount of these oxygen vacancies by some external actions, such as heating/annealing, gamma-irradiation and combined hydrogenation with microwave irradiations [23]. In any case the electron photoexcitation from additional energy levels which arose due to oxygen vacancy inside the forbidden band gap can provide this photocatalytic activity of such treated HAP samples.

## REFERENCES

- [1] B. D. Ratner, A. S. Hoffman, F.J. Schoen, J.E. Lemons, *Biomaterials Science*. 3rd ed. Oxford: Academic Press, (2013).
- [2] V. Bystrov, A. Bystrova, Yu. Dekhtyar, I. A. Khlusov, V. Pichugin, K. Prosolov, Yu. Sharkeev, Electrical functionalization and fabrication of nanostructured hydroxyapatite coatings. In: A. Iulian, eds. *Bioceramics and Biocomposites: From Research to Clinical Practice*. John Wiley & Sons, Inc., Hoboken, New Jersey, 149-190 (2019).
- [3] B. Leon, J. A. Janson, *Thin calcium phosphate coatings for medical implants*. Berlin: Springer, (2009).
- [4] M. Epple, K. Ganesan, R. Heumann, J. Klesing, A. Kovtun, S. Neumann and V. Sokolova, *J. Mater. Chem.* **20**, 18 (2010).
- [5] M. I. Kay, R. A. Young, A. S. Posner, *Nature* **204**, 1050 (1964).
- [6] S. Weiner, P. A. Price, *Calcif. Tissue Int.* **39**, 365 (1986).
- [7] Noriko Kanzaki, Kazuo Onuma, Atsuo Ito, Kay Teraoka, Tetsuya Tateishi, Sadao Tsutsumi, *J. Phys. Chem. B.* **102**, 6471 (1998).
- [8] V. S. Bystrov, *Math. Biol. Bioinform.* **12**, 14 (2017).
- [9] C.A. Santana, C.Piccirillo, S.I.A. Pereira, R.C.Pullar, S.M.Lima, P.M.L. Castro, *Journal of Environmental Chemical Engineering.* **7**(5), 103403 (2019).
- [10] N. Hitmi, C. LaCabanne, R. A. Young, *J. Phys. Chem. Solids.* **47** (6), 533 (1986).
- [11] S. Nakamura, H. Takeda, K. Yamashita, *J. Appl. Phys.* **89** (10), 5386 (2001).
- [12] S. A. M. Tofail, D. Haverty, K. T. Stanton, J. B. McMonagle, *Ferroelectrics.* **319**, 117 (2005).
- [13] S. A. M. Tofail, D. Haverty, F. Cox, J. Erhart, P. Hána, V. Ryzhenko, *J. Appl. Phys.* **105**(6), 064103 (2009).
- [14] S. A. M. Tofail, C. Baldisserri, D. Haverty, J. B. McMonagle, J. Erhart, *J. Appl. Phys.* **106**(10), 106104 (2009).
- [15] S. B. Lang, S. A. M. Tofail, A. A. Gandhi, M. Gregor, C. Wolf-Brandstetter, J. Kost, S. Bauer, M. Krause, *Appl. Phys. Lett.* **98**, 123703 (2011).
- [16] S. B. Lang, S. A. M. Tofail, A. L. Kholkin, M. Wojtaś, M. Gregor, A. A. Gandhi, Y. Wang, S. Bauer, M. Krause, A. Plecenik, *Sci. Rep.* **3**, 2215 (2013).
- [17] S. B. Lang, *Phase transitions*, **89** (78), 678694 (2016).
- [18] V.S. Bystrov, E. Paramonova, Yu. Dekhtyar, A. Katashev, A. Karlov, N. Polyaka, A.V. Bystrova, A. Patmalnieks, A.L. Kholkin, *J. Phys. Cond. Matter.* **23**, 065302 (2011).
- [19] V.S. Bystrov, J. Coutinho, A.V. Bystrova, Yu.D. Dekhtyar, R.C. Pullar, A. Poronin, E. Palcevskis, A. Dindune, B. Alkan, C. Durucan, *J. Phys. D Appl. Phys.* **48**, 195302 (2015).
- [20] V. S. Bystrov, *Ferroelectrics.* **475**, 148 (2015).
- [21] V. S. Bystrov, *Ferroelectrics.* **541**, 25 (2019).
- [22] H. Nishikawa, *Phosphorus Res. Bull.* **21**, 97 (2007).
- [23] V.S. Bystrov, E.V. Paramonova, Yu.D. Dekhtyar, A. V. Bystrova, R.C. Pullar, S. Kopyl, D.M. Tobaldi, C. Piccirillo, L.A. Avakyan, J. Coutinho, *Ferroelectrics.* **509**, 105 (2017).
- [24] V.S. Bystrov, C. Piccirillo, D.M. Tobaldi, P.M.L. Castro, J. Coutinho, S. Kopyl, R.C. Pullar, *Applied Catalysis B: Environmental.* **196**, 100 (2016).
- [25] L.A. Avakyan, E.V. Paramonova, José Coutinho, Sven Öberg, V.S. Bystrov, Lusegen A. Bugaevet, *J. Chem. Phys.* **148**, 154706 (2018).
- [26] V. S. Bystrov, L. A. Avakyan, E. V. Paramonova, J. Coutinho, *J. Chem. Phys.C.* **123**(8), 4856 (2019).
- [27] AIMPRO, (2010). [<http://aimpro.ncl.ac.uk/>] (Accessed February 2016).
- [28] VASP (Vienna Ab initio Simulation Package), [<https://www.vasp.at/>] (Accessed July 2019).
- [29] HyperChem:Tools for Molecular modeling (release 8). Gainesville: Hypercube, Inc. 2002.
- [30] C. Halperin, S. Mutchnik, A. Agronin, M. Molotskii, P. Urenski, M. Salai, G. Rosenman, *Nano Lett.*, **4** (7), 1253 (2004).
- [31] Shunbo Hu, Fanhao Jia, Cornelia Marinescu, Fanica Cimpoesu, Yuting Qi, Yongxue Tao, Alessandro Stroppa, Wei Ren, *RCS Adv.*, **7**, 21375 (2017).
- [32] Jennifer Vandiver, Delphine Dean, Nelesh Patel, William Bonfield, Christine Ortiz, *Biomaterials.* **26**, 271 (2005).
- [33] G.-X. Qian, R. M. Martin, D. J. Chadi, *Phys. Rev. B: Condens. Matter Mater. Phys.* **38**, 7649 (1988).
- [34] A. V. Bystrova, Yu. Dekhtyar, A. I. Popov, J. Coutinho, V.S. Bystrov, *Ferroelectrics* **475**(1), 135 (2015).
- [35] V. Bystrov, A. Bystrova, Yu. Dekhtyar, *Advances in Colloid and Interface Science* **249**, 213 (2017).